



Performance evaluation of pan position methods in domestic induction cooktops

Nihan Altintas¹ · Metin Ozturk^{2,3} · Ulas Oktay^{1,4}

Received: 19 July 2022 / Accepted: 17 April 2023 / Published online: 27 April 2023
© The Author(s), under exclusive licence to Springer-Verlag GmbH Germany, part of Springer Nature 2023

Abstract

The single-switch quasi-resonant inverter topology is typically favored for low-cost and low-output-power applications among the resonant inverters used in induction heating systems. Despite the low-cost advantage of the quasi-resonant inverter, the soft-switching range is quite narrow, and it is not stable depending on the electrical parameters of the load that is desired to be heated. In addition, to ensure safe operation in induction cookers, it is important to know the properties of the material from which the pan is made, the diameter of the pan, and the coverage ratio between the pan and the coil. Especially in the single-switch quasi-resonant topology, it is complicated to determine pan size and pan position compared to other topologies. On the other hand, closed-loop power control algorithms are essential for single-switch inverter applications. A big relationship exists between pan detection algorithms and closed-loop power control methods used. This study proposes six alternative methods of determining the pan–coil coverage ratio for the single-switch quasi-resonant topology used in domestic induction heating cooktops. Unlike state-of-the-art methods, the proposed methods do not increase the system's cost since they use the processor for power control, are not complicated, and provide ease of application. Each method is examined in a simulation environment and experimentally for different coverage rates and compared. As a result of the comparison, the diode conduction time method in single-switch quasi-resonant systems is the most appropriate regarding reliability and applicability.

Keywords Coil pan coverage · Domestic induction cooktops · Single switch topology · Pan detection methods

1 Introduction

Induction heating (IH) technology is widely used in many applications, especially domestic, industrial and medical, due to its features such as high reliability, high efficiency

Metin Ozturk and Ulas Oktay have contributed equally to this work.

✉ Nihan Altintas
naltin@yildiz.edu.tr
Metin Ozturk
metinozturk@esenyurt.edu.tr
Ulas Oktay
ulas.oktay@arcelik.com

- ¹ Electrical Engineering Department, Yildiz Technical University, 34220 Istanbul, Turkey
- ² Electrical-Electronics Engineering, Istanbul Esenyurt University, 34510 Istanbul, Turkey
- ³ Research Development Department, Mamur Technology Inc, 34590 Selimpasa, Istanbul, Turkey
- ⁴ Research Development Department, Arcelik Inc, 34950 Cayirova, Istanbul, Turkey

and rapid heating [1, 2]. The general power flow diagram of domestic induction cooktops (DIC) is given in Fig. 1a. Firstly, AC grid voltage is converted into DC voltage with the help of a rectifier. The rectified grid voltage applied to the input of the inverter is converted into a high-frequency AC voltage at the output of the inverter. By applying this voltage to the induction coil, a current that changes with time passes through the coil. With the current passing, a magnetic field creates in the coil that cuts the bottom of the pan. The voltage induced by the magnetic field in the pan causes eddy currents to flow through the bottom of the pan.

High-frequency current in induction hobs is obtained using different inverter topologies. In domestic IH applications are generally used half bridge series resonant (HBSR) and single-switch quasi-resonant (SSQR) topologies. HBSR topology is preferred in high-power home applications due to its design and control simplicity. In low-power applications, the SSQR topology, which has a lower cost compared to HBSR, is the best solution [3, 4].

The pan and induction coil pair are modeled as equivalent resistance R_{EQ} and equivalent inductance L_{EQ} in the equivalent electrical circuit of the induction cooker [5].

IH system performance; the diameter of the pan depends on many parameters such as the relative coverage ratio between the pan and the coil, the operating frequency of the circuit and the properties of the material from which the pan is made [6–8]. DIC are commonly designed for ferromagnetic cookware [9, 10]. In Fig. 1b, the frequency-dependent change of the switch current for pans using different materials is given at constant power and constant main voltage. Here, it is seen that currents can damage the switch, especially if there is no pan and when aluminum and copper pans are used. Using a non-ferromagnetic pan with high inductance and low resistance value may cause overheating and damage to the system. Therefore, for the electronic circuit to work safely, it is very important that it includes a control method that can detect the material properties of the pan (resistivity, magnetic permeability), the coverage ratio between pan and coil, the diameter of the pan, and the presence or absence of the pan.

In DIC, the presence of the load is determined by measuring the damping factor. Long oscillation signals are detected when there is no load on the coil. A few cycles damped oscillation signal is detected when the metal load is placed on the coil [11]. This method is useful for detecting the presence of a load. However, this method cannot determine load exact position between the load and the coil.

To understand the different induction loads, lots of methods are used and improved in the literature [12, 13]. In [14, 15], temperature sensors and phase-sensitive detector (PSD) are used for load recognition, respectively. The pan coverage ratio is defined in [16] with the help of a convolutional neural network using the output power, current and quality factor. In [17], pan type and size recognition based on equivalent impedance estimation using machine learning has been proposed. Online impedance estimation based on the first harmonic coefficients of the discrete-time Fourier series (DTFS) of the measured output voltages and currents of the converter using FPGA is proposed in [18]. In the load identification method presented in [19], the quality factor is used, which is found by analyzing analytical expressions with the help of FPGA using the resonant capacitor voltage measured using passive components and ADC. PSD algorithm is proposed to determine equivalent resistance and equivalent inductance values from converter voltage and current waveforms with FPGA [20]. DTFS coefficients of the converter output voltage and load current used in the load identification are calculated by the FPGA by taking the first-order $\Sigma - \Delta$ directly from the analog-to-digital converter output [21]. In [22], the resonant capacitor voltage is measured, and the harmonic components of the voltage are obtained with the help of FPGA to be used in load estimation. Pan recogni-

tion by such methods increases the cost of the system, while at the same time complicates the control and is not practical in industrial application.

Almost all of the studies in the literature are applied to DIC that HBSR is used [23]. Determining the pan size and pan-coil coverage ratio in SSQR is more complex than in HBSR, and therefore there is a few research in the literature [24, 25]. The main reason for this is that the relationship between the closed-loop power control algorithm and the pot recognition methods is much more pronounced in the SSQR and the safe operating limits of the SSQR are very narrow. In [24], the neural network is applied to estimate the pan size by calculating the power factor and the absolute value of the impedance for the first four harmonics of the SSQR converter's switching frequency. Since the variation of the equivalent impedance of the materials is not taken into account here, depending on the excitation level, problems may occur in the converter under different operating conditions. In the study proposed in [25], it is not possible to apply it practically because very small time intervals need to be determined. However, this study has some disadvantages compared to the proposed study. At the beginning of these disadvantages are using some analog and digital circuit elements, using a highly skilled microprocessor or microcontroller, and developing complex algorithms. Moreover, even if all costs are covered, measurement errors in the order of $nsec$ may cause the R_{EQ} and L_{EQ} values to be calculated differently than they should be. As a result, there is a research gap in the literature on pan detection in SSQR converters, which are increasingly used in flexible DICs.

The closed-loop power control algorithms are essential for SSQR inverter applications [26–30], and there is a big relationship between pan detection algorithms and closed-loop power control methods used. It means that the controller has to control not only output power, but also relative positions between pan and coil. Otherwise, the controller cannot detect the load change and inverter circuit can be damaged because of the over voltage, over current or over heat. Basically, two closed-loop power control methods are used in SSQR inverter. These control methods are based on controlling the maximum switch voltage V_{CEmax} and the maximum coil current I_{LEQmax} .

In this study, new three pan detection methods are proposed for SSQR converters. Each of these methods is available for cases of controlling the output power with the help of switch voltage or coil current. As a result, six alternative methods of determination of pan coil coverage ratio are proposed, compared and analyzed for the SSQR topology used in a DIC. The main benefit of the proposed methods is that the SSQR converter is operated with different ferromagnetic properties load without problems. In addition, compared to the limited number of studies on SSQR in the literature, cost-effective implementation is carried out. The proposed methods are implemented using existing micro-

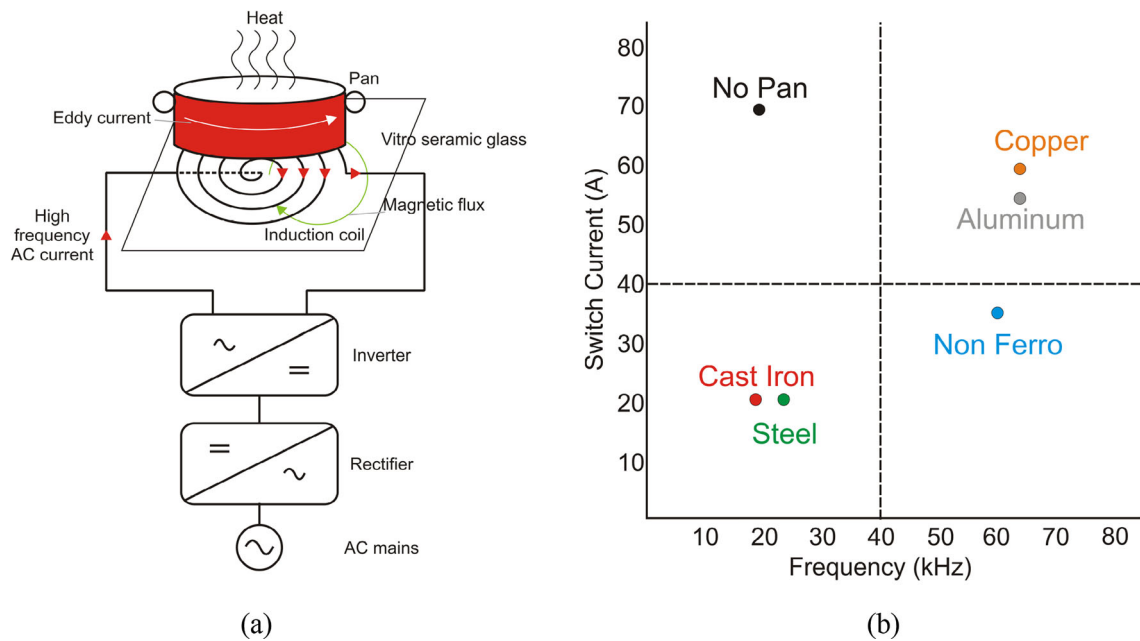


Fig. 1 a Basic principle of IH, b switch current-frequency for various pan materials

controller used for power control and are not increased the system cost. Here, three pans with different ferromagnetic properties are used as a load: stainless steel, cast iron and granite.

All proposed methods for each loads were analyzed and compared in simulation and experimental. Also, these methods are examined in terms of ease of application and reliability. From the results, it has been determined that the reverse parallel diode conduction time method gives more accurate results than the switch voltage and input voltage comparison method, while the maximum switch voltage/coil current method depends on the operating conditions such as voltage and power level of converter. Moreover, in order for the maximum current/voltage method to work properly, some reference values must be obtained first. In order for reference values to be formed, the power transferred to the pan must become stable. Steady-state analysis and determination of reference values are not easy and require some compelling software algorithms. In SSQR systems, the reverse parallel diode conduct time method is the most suitable method for both power control methods in terms of reliability and applicability, since it gives accurate results without steady-state formation, does not change according to the input voltage and power transferred to the pan.

The rest of this article is organized as follows. Section 2 details the basic principle of induction heating systems. The circuit of the SSQR inverter used in the DIC, operating modes and the main equations describing the circuit operation are given in Sect. 3. In Sect. 4, proposed pan detection methods are given for both closed-loop power control meth-

ods. A detailed system control of the DIC with pan detection methods is given in Sect. 5. Section 6 details simulation and experimental results. The main experimental waveforms are presented and discussed, proving the feasibility of the proposed methods. Finally, Sect. 7 concludes this article.

2 Basic principle of induction heating systems

When an alternating current is applied to a coil, a magnetic field is created around the coil according to Faraday’s law given in (1)–(3).

$$F = \int H \cdot dl \tag{1}$$

Here, magneto motor force (F), magnetic field (H), length of the infinitesimal line element (dl).

$$\phi = \mu \cdot H \cdot A \tag{2}$$

Here, magnetic flux (ϕ), permeability of material (μ), cross-section area (A).

$$E = -N \cdot d\phi/dt \tag{3}$$

Here, electromotive force (E), number of turns (N).

The velocity of the magnetic movement changes due to an object placed in a magnetic field. The magnetic field density decreases as the object moves away from the surface toward

the center. Faraday’s law states that there is an inverse relationship between the current produced on the surface of a conductive object and the current in the inducing circuit. Currents passing through the surface of the object create an eddy current [5]. Due to the skin effect, which is formulated in (4)–(6), the penetration current through the bottom of the pan will be decreased. The current density (i_x) at the x point is given in (4). It is seen that the current density depends on the current density at the surface (i_0) and frequency-dependent skin depth factor (d_0). The expression of the skin depth factor is given in (5). In this expression, ω is angular frequency of current, ρ is resistivity and μ is relative magnetic permeability. The expression of the penetration depth δ is given in (6). It varies greatly depending on the current frequency (f). The equation expressing the surface resistance of the pan (R_p) is given in (7).

$$i_x = i_0 \cdot e^{-x/d_0} \tag{4}$$

$$d_0 = \sqrt{\frac{2 \cdot \rho}{\mu \cdot \omega}} \tag{5}$$

$$\delta = \sqrt{\frac{1}{4\pi^2 \cdot 10^{-7}} \cdot \frac{\rho}{f \cdot \mu_r}} \tag{6}$$

$$R_p = \frac{\rho}{\delta} = \sqrt{4\pi^2 \cdot 10^{-7}} \cdot \sqrt{f \cdot \mu_r \cdot \rho} \tag{7}$$

In order to simulate DIC systems, a model should be created by assuming that there is a cooking pan on the coil. Transformer is generally used as the equivalent model of this system [31].

A physical model of the induction coil with pan is given in Fig. 2a. Here, resistance and inductance of the induction coil are indicated by R_c and L_c , respectively. Magnetic coupling between the coil and the pan is defined with mutual inductance M . Resistance and inductance of the pan are represented with R_p and L_p , respectively [31]. The simplified model when all the quantities are referring to coil side is given in Fig. 2b. Here, R_{ps} and L_{ps} indicate that coil side pan parameters. The equivalent electrical circuit of the induction cooktop is given in Fig. 2c. The equations of R_{EQ} and L_{EQ} are given in (8) and (9).

$$R_{EQ} = R_c + R_{ps} = R_c + \frac{4\pi^2 f^2 M^2 R_p}{R_p + 4\pi^2 f^2 L_p^2} \tag{8}$$

$$L_{EQ} = L_c + L_{ps} = L_c - \frac{4\pi^2 f^2 M^2 R_p}{R_p + 4\pi^2 f^2 L_p^2} \tag{9}$$

The value of M varies depending on the coverage ratio between pan and coil. As can be seen from (8) and (9), when the M value increases, the R_{EQ} value increases, while the L_{EQ} value decreases. The opposite is true when M value decreases.

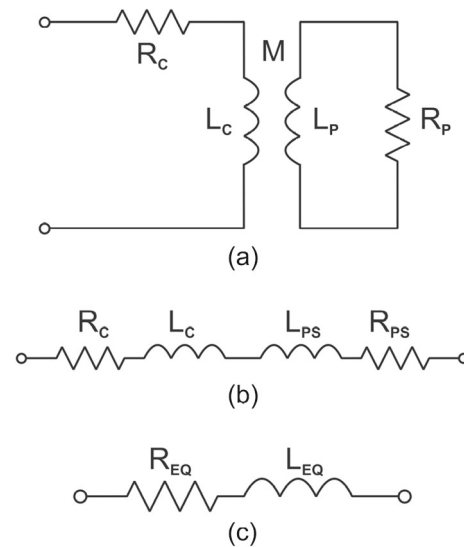


Fig. 2 Models of pan and induction coil **a** physical, **b** simplified, **c** equivalent

3 Circuit description

The equivalent circuit of the SSQR inverter used in a DIC is presented in Fig. 3. The inverter circuit consists of the switch T , a diode in reverse parallel to the switch (called a freewheeling diode) D , resonance capacitor C_{RES} , equivalent series resistance R_{EQ} and inductance L_{EQ} .

Four stages occur in one switching cycle of SSQR inverter in the steady-state operation. In Fig. 4, the equivalent circuit schemes of the operation modes are given, respectively. The waveforms concerning the operation stages are shown in Fig. 5. A detailed analysis of every stage is presented below.

Stage I (t_6-t_0 : Fig. 4a): At the beginning of the interval the switch T is off state. When the control signal of the switch is applied, T is turned on with zero voltage (ZVT) transitions.

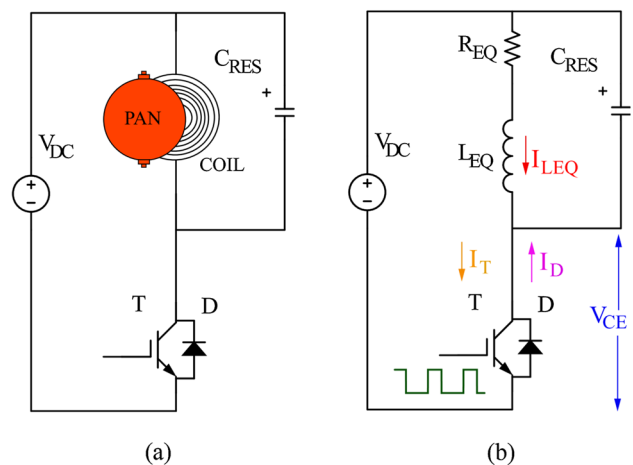


Fig. 3 **a** Circuit scheme of DIC with SSQR inverter, and **b** equivalent circuit

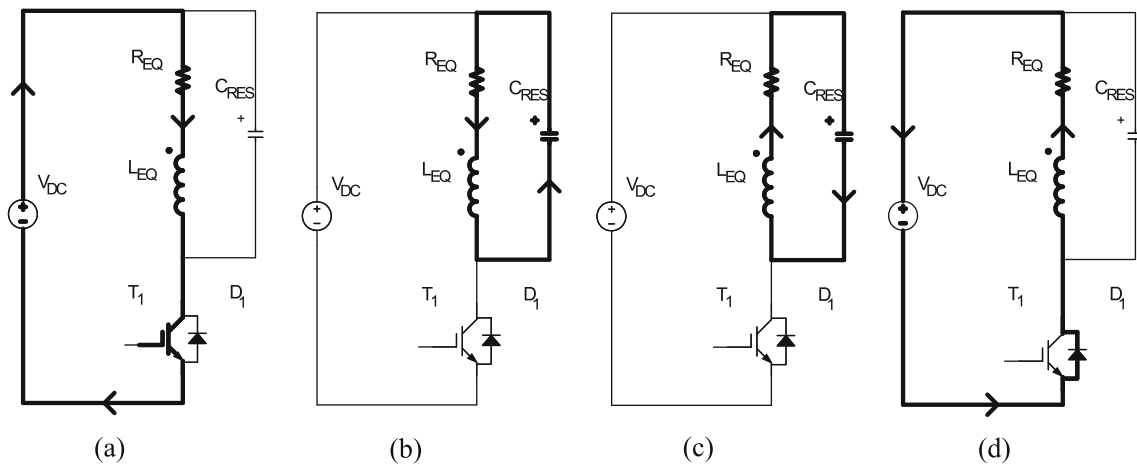


Fig. 4 Equivalent circuit schemes of the operation modes of SSQR

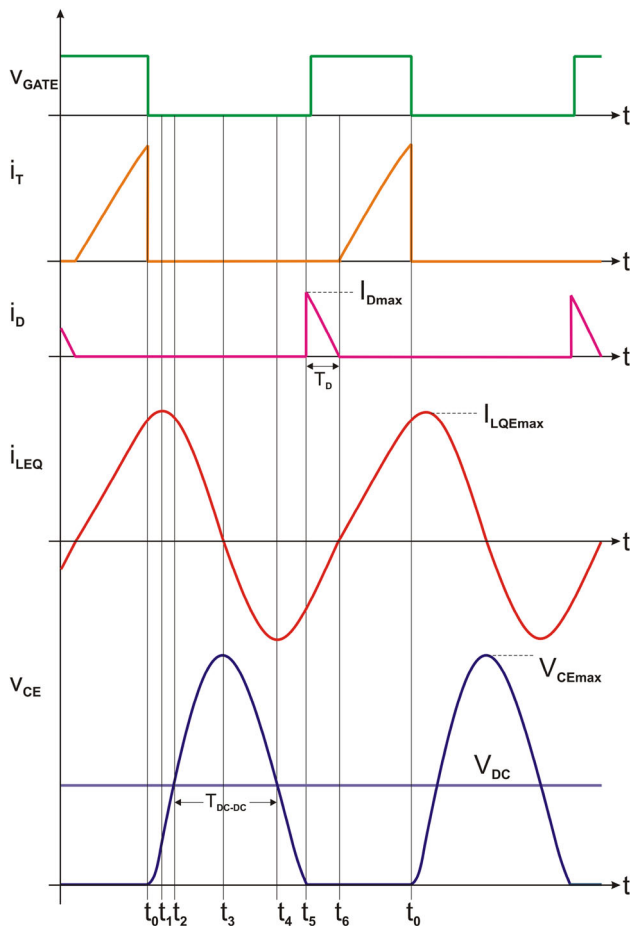


Fig. 5 Current and voltage waveforms of SSQR

In general, the circuit behaves like a series RL circuit while the T switch is on state. During time t_{ON} , energy is stored in the coil due to the current flowing through the RL circuit. For this stage, the current equations of equivalent inductance

can be written as in (10)–(12).

$$i_{LEQ}(0) = 0 \tag{10}$$

$$i_{LEQ}(t) = i_T(t) = \frac{V_{DC}}{R_{LEQ}} \cdot \left(1 - e^{-\frac{R_{LEQ}}{L_{LEQ}} \cdot t} \right) \tag{11}$$

$$V_{DC} = V_{LEQ} + V_{REQ} \tag{12}$$

Stage II–III (t_0 – t_5 : Fig. 4b, c): A series resonant occurs between R_{EQ} , L_{EQ} and C_{RES} in this stage, when the control signal of the switch T is removed. The circuit formed in this stage can be examined as a series RLC circuit. Energy transfer occurs between the resonant capacitor and the coil. The resonant capacitor voltage V_{CRES} reaches its maximum value V_{CEmax} and discharges to zero with continued resonance. The equations of I_{LEQ} are given in (13)–(20).

$$\alpha = \frac{R_{EQ}}{2L_{EQ}} \tag{13}$$

$$\omega_0 = \frac{1}{\sqrt{L_{EQ}C_{RES}}} \tag{14}$$

$$\omega_d = \sqrt{\omega_0^2 - \alpha^2} \tag{15}$$

$$T_{RES} = 2\pi\sqrt{L_{EQ}C_{RES}} \tag{16}$$

Here, α is damping coefficient, ω_0 is resonant frequency, ω_d is damped resonant frequency and T_{RES} is resonant period.

$$i_{LEQ}(t) = e^{-\alpha t} (B_1 \cos(\omega_d t) + B_2 \sin(\omega_d t)) \tag{17}$$

$$\begin{aligned} \frac{di_{LEQ}(t)}{dt} = & -e^{-\alpha t} [(B_1\omega_d + B_2\alpha) \sin(\omega_d t) \\ & + (B_1\alpha - B_2\omega_d) \cos(\omega_d t)] \end{aligned} \tag{18}$$

$$i_{LEQ}(0) \Rightarrow B_1 = I_0 \tag{19}$$

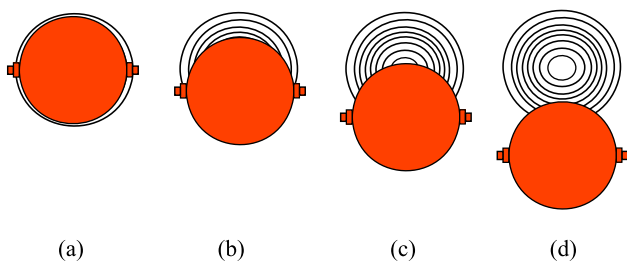


Fig. 6 Coverage ratio between pan and coil **a** 100% coupling. **b** 75% coupling. **c** 50% coupling. **d** 25% coupling

$$di_{LEQ}/dt \Rightarrow B_2 = (V_{DC} - R_{EQ}I_0)/(L_{EQ}\omega_d) + (\alpha I_0)/\omega_d \quad (20)$$

In addition, (21)–(24) can be used to calculate V_{CE} ,

$$v(t) = V_{DC} + e^{-\alpha t}(A_1 \cos(\omega_d t) + A_2 \sin(\omega_d t)) \quad (21)$$

$$dv(t)/dt = -e^{-\alpha t}[(A_1\omega_d + A_2\alpha) \sin(\omega_d t) + (A_1\alpha - A_2\omega_d) \cos(\omega_d t)] \quad (22)$$

$$v(0) \Rightarrow A_1 = -V_{DC} \quad (23)$$

$$dv_0/dt \Rightarrow A_2 = (I_0)/(C_{RES} - \alpha V_{DC})/\omega_d \quad (24)$$

Stage IV (t_5 – t_6 ; Fig. 4d): This interval starts with the turning on D diode which is placed the switch. The remaining energy in the equivalent inductance is transferred to the source with the help of the diode D. The switch is ideally turned on again when the diode is on state.

4 Pan detection methods

The relative positions between the pan and the coil used in this study are given in Fig. 6. Regardless of the ferromagnetic character of the pan used, to ensure reliability of the inverter circuit and reliable power control, the coverage ratio between the pan and the coil must be greater than a specified value. Otherwise, if the coverage ratio is smaller than the specified value during the operation, the current passing through the switch or the voltage values across the switch can be increase and the inverter circuit may be damaged. It is not easy to determine and control the boundary conditions in practical life, as the position of the pan on the coil, which is the complementary of the circuit in DIC, is determined by the user. As a result of this, the boundary conditions for each pan detection method are evaluated independently and trying to find best method for each kind of pans.

4.1 Power control with constant voltage V_{CEmax}

The resonant capacitor voltage provides essential information regarding the output power and soft switching conditions [27, 32]. In SSQR inverter used in induction cooktop applications, monitoring V_{CEmax} can be selected to control output power. When the monitoring V_{CEmax} to control output power, three different pan detection methods can be used to understand relative pan position.

4.1.1 Maximum coil current I_{LEQmax}

As a result of the usage of V_{CEmax} for closed-loop power control, I_{LEQmax} value can be used to understand relative pan position. It is very important to define the boundary conditions in the design process of the SSQR converter circuit. In stage II and stage III, series resonant circuit, I_{LEQ} and V_{CE} reaches their maximum values at $t = t_1$ and $t = t_3$, respectively. Knowing these two values is important in obtaining safe operation and in controlling system parameters such as power. As it can be seen from Fig. 5 that when I_{LEQ} reach its peak value I_{LEQmax} , the derivation of I_{LEQ} is equal to zero ($t = t_1$). As result of this I_{LEQmax} can be derived by the help of (25)–(27).

$$di_{LEQ}(t_1)/dt = 0 \Rightarrow i_{LEQ}(t_1) = I_{LEQmax} \quad (25)$$

$$t_1 = \tan^{-1}[-(B_1\alpha - B_2\omega_d)/(B_1\omega_d + B_2\alpha)] \quad (26)$$

$$I_{LEQmax} = i_{LEQ}(t_1) = e^{-\alpha t_1}(B_1 \cos(\omega_d t_1)) + (B_2 \sin(\omega_d t_1)) \quad (27)$$

4.1.2 Comparing V_{CE} and V_{DC}

With the series resonant between L_{EQ} and C_{RES} in the circuit, V_{CE} becomes equal to the DC source voltage V_{DC} at t_2 and t_4 . From (28)–(31) and Fig. 5, T_{RES} and ω_d can be derived easily. So a pan position method can be derived from the comparing V_{CE} and V_{DC} [33]. The interval t_{42} is expressed as the power switch DC-DC time in (32). If the pan is removed, the values of the L_{EQ} and R_{EQ} circuit components will change. The coil’s equivalent inductance L_{EQ} will be increased and the equivalent resistance will be decreased. In this case, the effect of equivalent resistance is negligible and the T_{DC-DC} is assumed to be approximately half of the resonant period. T_{DC-DC} increases with increasing L_{EQ} .

$$v(t_2, t_4) = V_{DC} \quad (28)$$

$$v(t_2) = V_{DC} + e^{-\alpha t_2}(A_1 \cos(\omega_d t_2) + A_2 \sin(\omega_d t_2)) \quad (29)$$

$$t_2 = \frac{\tan^{-1}(-A_1/A_2)}{\omega_d} \quad (30)$$

$$t_4 = t_2 + \frac{\pi}{\omega_d} \tag{31}$$

$$T_{DC-DC} = \frac{T_{RES}}{2} = \frac{\pi}{\omega_d} = \pi \sqrt{L_{EQ} C_{RES}} \tag{32}$$

4.1.3 Reverse-parallel diode conduction time

The diode D, which turns on when the capacitor voltage drops to zero at $t = t_5$ as seen from Fig. 5, ensures the return of the remaining energy in the inductance to the source. During the transfer of energy stored in L_{EQ} , diode D is forward-biased. The stored energy level changes depending on the pan feature. Parallel to this, since the conduction time of the diode will change, it gives important information for the detection of the presence of the pan.

The following equations are obtained by arranging the equations in (17)–(20) for the RL operating range of the circuit. The conduction time of the diode and the maximum value of the diode current are indicated by T_D and I_{Dmax} , respectively. T_D highly depends on L_{EQ}/R_{EQ} ratio. So, T_D can be used for pan detection in induction cooktops where SSQR topology is used.

$$-i_{LEQ}(t) = \frac{V_{DC}}{R_{EQ}} + \left(i_{LEQ}(t_5) - \frac{V_{DC}}{R_{EQ}} \right) e^{-\frac{R_{EQ}}{L_{EQ}}t} \tag{33}$$

$$i_{LEQ}(T_D) = 0 = \frac{V_{DC}}{R_{EQ}} + \left(I_{Dmax} - \frac{V_{DC}}{R_{EQ}} \right) e^{-\frac{R_{EQ}}{L_{EQ}}T_D} \tag{34}$$

$$T_D = -\frac{L_{EQ}}{R_{EQ}} \ln \left(1 + \frac{I_{Dmax}}{V_{DC}/R_{EQ} - I_{Dmax}} \right) \tag{35}$$

4.2 Power control with constant current I_{LEQmax}

In SSQR inverter application, monitoring I_{LEQmax} can be selected to control output power. In this case, three different pan detection methods can be used.

4.2.1 Maximum switch voltage V_{CEmax}

In induction cooktops using an SSQR inverter, the maximum power level at which the converter can operate is limited, depending on the breakdown voltage of the switch. When the I_{LEQ} current is zero, the switch voltage V_{CE} reaches its maximum value V_{CEmax} at t_3 . As result of this, V_{CEmax} can be derived by the help of (36)–(38).

$$i_{LEQ}(t_3) = 0 \Rightarrow v(t_3) = V_{CEmax} \tag{36}$$

$$t_3 = \tan^{-1}(-B_1/B_2)/\omega_d \tag{37}$$

$$V_{CEmax} = v(t_3) = V_{DC} + e^{-\alpha t_3} (A_1 \cos(\omega_d t_3) + A_2 \sin(\omega_d t_3)) \tag{38}$$

V_{CE} occurs during off period of T and I_{LEQ} can be measured continuously (32). It is seen from (21)–(24) that there is a big relationship between V_{CE} and I_{LEQ} . As a result of the usage of I_{LEQmax} for closed-loop power control, V_{CEmax} can be used to understand relative pan position.

4.2.2 Comparing V_{CE} and V_{DC}

As in the method of monitoring and controlling V_{CEmax} , V_{CE} and V_{DC} comparison can be used in this method for pan detection. As given above, it is not described again here. The applied circuit schematic to compare V_{CE} and V_{DC} is given in Fig. 7.

4.2.3 Reverse-parallel diode conduction time

As in the method of monitoring and controlling V_{CEmax} , the diode current conduction time T_D can be in this method for pan detection. As given above, it is not described again here.

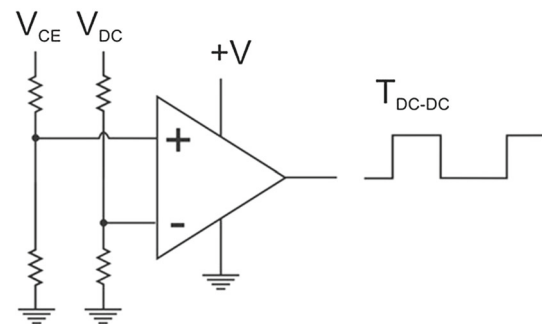


Fig. 7 Circuit schematic to compare V_{CE} and V_{DC}

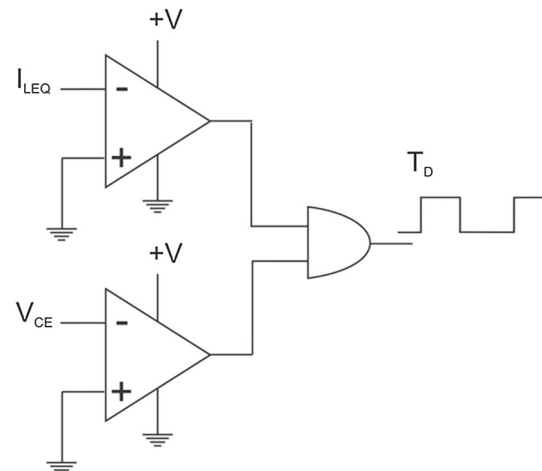


Fig. 8 Circuit schematic to get diode conduction time T_D

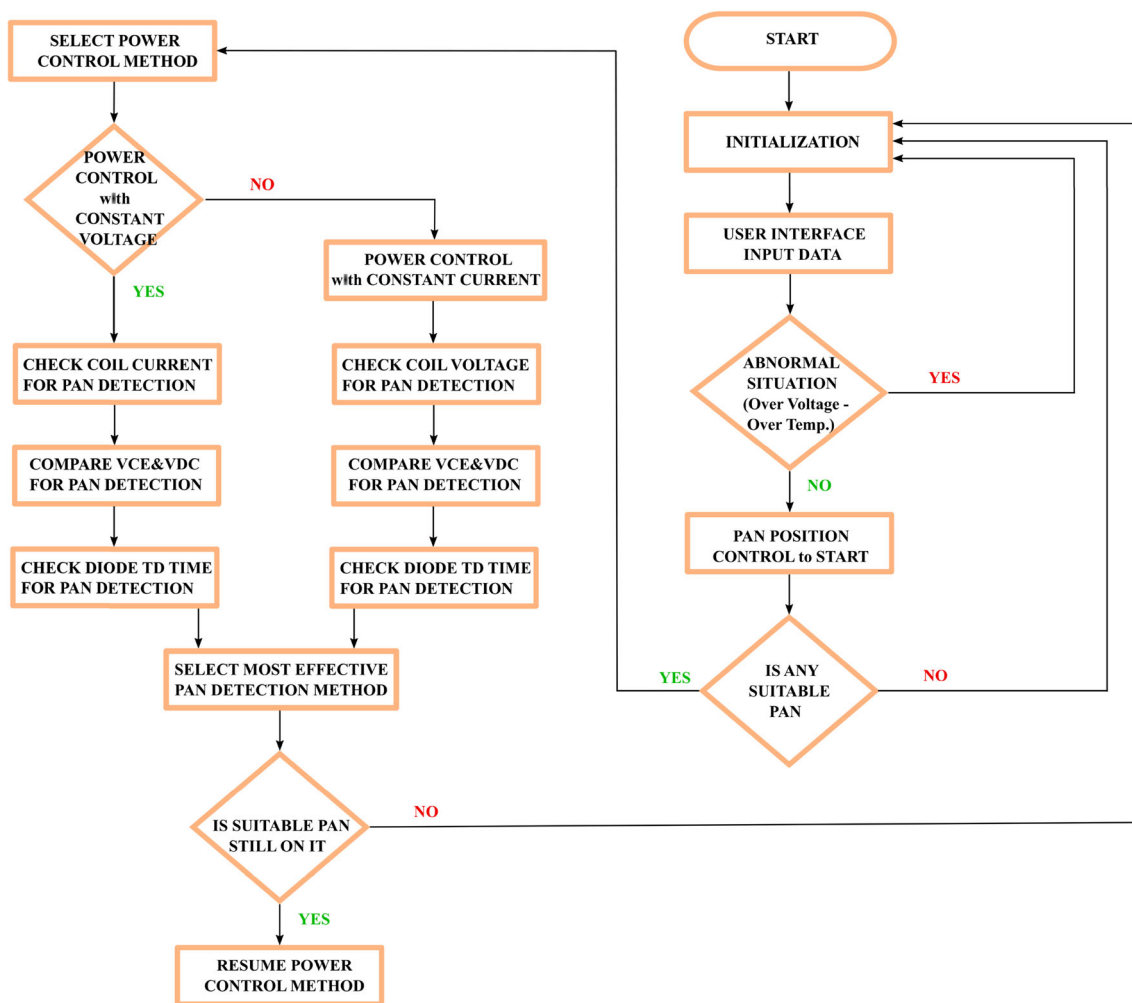


Fig. 9 Detailed system control loop for DIC

The applied circuit schematic to get diode conduction time T_D is given in Fig. 8.

5 System control with pan detection methods

The closed-loop power control algorithms are essential for SSQR inverter applications, and there is a big relationship between pan detection algorithms and closed-loop power control methods used. It means that the controller not only have to control output power, but also relative positions between pan and coil. Using the V_{CE} voltage to control the output power is preferable for its low cost and ease of use. Additional current reading elements are needed to control the output voltage using the I_{LEQ} current. Current reading method can be preferred in usage areas where cost is not important. Control algorithms in which both I_{LEQ} current

and V_{CE} voltage are used together will be the most reliable methods. For example, if the control is done with current and the V_{CE} voltage is above a certain value, it can be an ideal method to control with voltage. In addition to all this, the overall control loop of the DIC depends on different parameters such as input voltage and temperature, in addition to metal detection and power control. Detailed system control loop is given in Fig. 9.

With the help of the user interface, the control process begins with the determination of the power to be transferred to the pan. If there is no abnormal situation such as high temperature and high voltage, it is questioned whether there is a pan with suitable ferromagnetic properties in the product. With the detection of the presence of the pan, the power control and pan detection work, which is the subject of the article, begins. It is extremely important that the pan remains on the product even after the heating process has started.

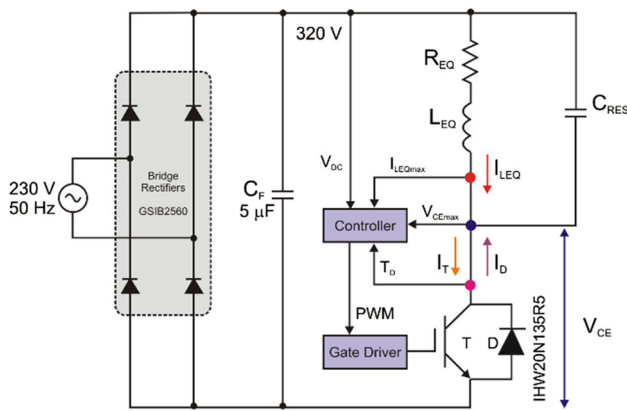


Fig. 10 The experimental circuit scheme

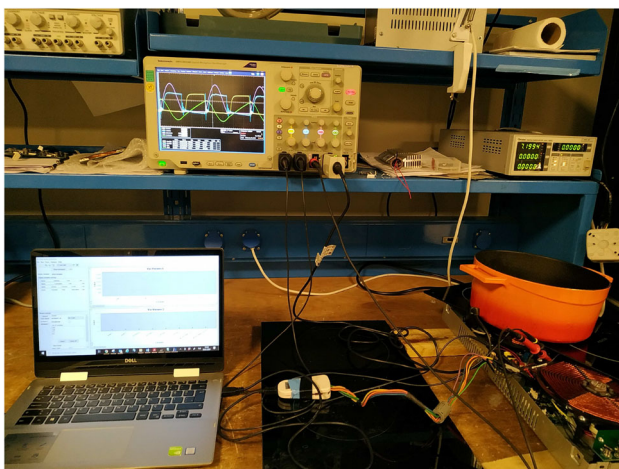


Fig. 11 The photographs of experimental setup

6 Simulation and experimental verifications

The theoretical analysis of six different pan detection methods proposed for DIC systems using the SSQR inverter topology is given above. In this section, the theoretical analysis of the proposed pan detection methods has been verified with simulation and experimental circuits. The circuit diagram of the induction cooktops using the SSQR topology is given in Fig. 10. Photographs of the circuit board and experimental setup are shown in Fig. 11. Input AC voltage and frequency $V_{AC} = 230 \text{ V}$, $f = 50 \text{ Hz}$, the input power $P_{IN} = 2000 \text{ W}$ and DC voltage $V_{DC} = 320 \text{ V}$. The single-phase integrated bridge rectifier GSIB2560 is used to convert input AC voltage to DC voltage. For enhanced reliability, IHW20N135R5 IGBT with a high breakdown voltage of 1350 V and a rated current of 20 A is used as the main switch. No additional diode is used since it has a switch body diode. The reference coil and pan diameter are 180 mm and $C_{RES} = 270 \text{ nF}$. Three ferromagnetic pans with different

characteristics are used as loads in simulation and experimental studies. First one is stainless steel pan, second one is cast iron pan, and the last one is granite pan with stainless steel base. The inductance L_{EQ} and the resistance R_{EQ} values are varied according to the relative position between the reference pan and the coil. L_{EQ} and R_{EQ} values for four different coverage ratios and three different pans were measured with the GwInstek LCR-821 LCR meter at a frequency of 20 kHz and are given in Table 1. Analyses are carried out using the values in Table 1.

Three different pans that have different ferromagnetic specifications are analyzed depend on pan position and power control methods. The main purpose is to determine the safe working limits for all kind of pans that can be used in induction hob system. Firstly, the theoretical analysis of the proposed pan detection methods has been carried out with simulations and the results are verified with experimental results.

As shown in Tables 2, 4 and 6, I_{LEQmax} , T_{DC-DC} and T_D values change at constant V_{CEmax} are listed to understand the pan movement from 100% coverage to 0%. Likewise, Tables 3, 5 and 7 show the V_{CEmax} , T_{DC-DC} and T_D values change at constant I_{LEQmax} .

As with other inverter applications, the semiconductor collector voltage level must not exceed the breakdown voltage given in the catalog for the SSQR inverter application. Otherwise, the semiconductor and inverter circuit can be easily damaged. Increasing the break down voltage level helps to protect the semiconductor from overvoltage, but causes increased conduction and switching losses. Hence, for every design there is an optimum point between losses and overvoltage protection. In SSQR inverter application for home appliances, 1200 V DC is the optimum breakdown voltage level and the safe working conditions for all kind of ferromagnetic pans are limited with 1200 V DC V_{CE} value.

To measure the pulse width of the T_{DC-DC} , a comparator with input variables V_{DC} voltage and V_{CE} voltage can be used. Similarly, to measure the T_D conduction time, the zero crossing of the IGBT current (t_6) and the zero crossing of the V_{CE} voltage (t_5) can be compared using various electronic methods. On the other hand, the transmission time of the diode current ($t_6 - t_5$) can be measured directly.

From Tables 2, 3, 4, 5, 6 and 7, six different pan detection methods can be used to understand the pan relative position, regardless of the control method and pan specifications. However, the most effective way to understand load changing is T_D value change ratio at constant I_{LEQmax} . To protect the semiconductor from over voltage $\Delta T_D = 80\%$ value can be a boundary condition for different kind of pans. In addition to use ΔT_D , if the coil current is used as power control method, the limit value of ΔT_D can be also defined for boundary conditions. $\Delta T_D \leq 11 \mu\text{s}$ can be used for safe working conditions for all kind of ferromagnetic pans.

Table 1 R_{EQ} and L_{EQ} values of inverter circuit

Pan and coil	Stainless steel		Cast iron		Granite pan	
	R_{EQ} (Ω)	L_{EQ} (μH)	R_{EQ} (Ω)	L_{EQ} (μH)	R_{EQ} (Ω)	L_{EQ} (μH)
0%	0.16	114.1	0.16	114.1	0.16	114.1
25%	1.03	109.48	0.99	113.85	0.32	103.03
50%	2.35	95.49	3.05	105.47	0.67	93.43
75%	3.12	83.84	3.93	94.07	1.04	73.01
100%	3.36	81.81	4.21	89.76	1.48	69.07

Table 2 I_{LEQmax} , T_{DC-DC} and T_D values change at constant V_{CEmax}

Pan and coil coverage	V_{CEmax} (V)	I_{LEQmax} (A)	ΔI_{LEQmax} (%)	T_{DC-DC} (μS)	ΔT_{DC-DC} (%)	T_D (μS)	ΔT_D (%)
<i>Equation and simulation results for stainless steel pan</i>							
0%	925	29	27.5%	17.44	17.6%	9.01	54.8%
25%	925	31	22.5%	17.09	15.2%	8.47	45.5%
50%	925	35	12.5%	15.98	7.8%	7.15	22.9%
75%	925	39	2.5%	15.01	1.2%	6.10	4.8%
100%	925	40	REF	14.83	REF	5.82	REF

Table 3 V_{CEmax} , T_{DC-DC} and T_D values change at constant I_{LEQmax}

Pan and coil coverage	V_{CEmax} (V)	I_{LEQmax} (A)	ΔI_{LEQmax} (%)	T_{DC-DC} (μS)	ΔT_{DC-DC} (%)	T_D (μS)	ΔT_D (%)
<i>Equation and simulation results for stainless steel pan</i>							
0%	1142	40	23.5%	17.44	17.6%	13.18	126.5%
25%	1096	40	18.5%	17.09	15.2%	11.87	103.9%
50%	1000	40	8.1%	15.98	7.8%	8.67	48.9%
75%	928	40	0.3%	15.01	1.2%	6.16	5.8%
100%	925	40	REF	14.83	REF	5.82	REF

Table 4 I_{LEQmax} , T_{DC-DC} and T_D values change at constant V_{CEmax}

Pan and coil coverage	V_{CEmax} (V)	I_{LEQmax} (A)	ΔI_{LEQmax} (%)	T_{DC-DC} (μS)	ΔT_{DC-DC} (%)	T_D (μS)	ΔT_D (%)
<i>Equation and simulation results for Cast iron pan</i>							
0%	870	27.09	26.1%	17.44	12.1%	7.97	77.1%
25%	870	28.21	23.1%	17.42	11.9%	7.66	70.2%
50%	870	31.79	13.3%	16.81	7.9%	6.06	34.7%
75%	870	35.31	3.7%	15.92	2.2%	4.95	10.0%
100%	870	36.65	REF	15.57	REF	4.5	REF

Table 5 V_{CEmax} , T_{DC-DC} and T_D values change at constant I_{LEQmax}

Pan and coil coverage	V_{CEmax} (V)	I_{LEQmax} (A)	ΔI_{LEQmax} (%)	T_{DC-DC} (μS)	ΔT_{DC-DC} (%)	T_D (μS)	ΔT_D (%)
<i>Equation and simulation results for cast iron pan</i>							
0%	1070	36.65	22.9%	17.44	12.1%	11.81	162.4%
25%	1044	36.65	20.0%	17.42	11.9%	11.06	145.8%
50%	956	36.65	9.9%	16.81	7.9%	7.83	74.0%
75%	892	36.65	2.5%	15.92	2.2%	5.37	19.3%
100%	870	36.65	REF	15.57	REF	4.5	REF

Table 6 I_{LEQmax} , T_{DC-DC} and T_D values change at constant V_{CEmax}

Pan and coil coverage	V_{CEmax} (V)	I_{LEQmax} (A)	ΔI_{LEQmax} (%)	T_{DC-DC} (μ S)	ΔT_{DC-DC} (%)	T_D (μ S)	ΔT_D (%)
<i>Equation and simulation results for granite pan</i>							
0%	982	32.39	27.5%	17.44	28.4%	10.11	37.9%
25%	982	34.44	22.9%	16.57	22.1%	9.60	30.9%
50%	982	36.69	17.8%	15.78	16.2%	8.99	22.6%
75%	982	42.43	4.9%	13.96	2.8%	7.77	6.0%
100%	982	44.65	REF	13.58	REF	7.33	REF

Table 7 V_{CEmax} , T_{DC-DC} and I_{LEQmax} values change at constant I_{LEQmax}

Pan and coil coverage	V_{CEmax} (V)	I_{LEQmax} (A)	ΔI_{LEQmax} (%)	T_{DC-DC} (μ S)	ΔT_{DC-DC} (%)	T_D (μ S)	ΔT_D (%)
<i>Equation and simulation results for granite pan</i>							
0%	1233	44.65	25.6%	17.44	28.4%	14.89	103.1%
25%	1180	44.65	20.1%	16.57	22.1%	13.20	80.1%
50%	1128	44.65	14.9%	15.78	16.2%	11.60	58.3%
75%	1018	44.65	3.7%	13.96	2.8%	8.34	13.8%
100%	982	44.65	REF	13.58	REF	7.33	REF

The waveforms taken from the application circuit for the use of the I_{LEQmax} method and for two different coverage ratios are given in Fig. 12a–f. In Fig. 12a, b, I_{LEQ} and V_{CE} waveforms are given for the stainless-steel pan. The results obtained for 100% coverage ratio are given in Fig. 12a and for 25% which is the boundary coverage ratio value are given in Fig. 12b. In Fig. 12a, it is seen that the conduction time of the diode is very low. After the capacitor voltage reaches the V_{DC} voltage, the negative coil current drops to zero in a very short time. As can be seen from figure, the control signal of the switch is applied in the conduction time interval of the diode and the switch is turned on under soft switching. The maximum value of the voltage across the switch is nearly 950V. In Fig. 12b, it is seen that the conduction time of the diode increases with the decrease of the coverage ratio. In this case, V_{CEmax} , T_D and T_{DC-DC} values increased by 15, 78%, 100% and 13, 80%, respectively.

The I_{LEQ} and V_{CE} waveforms are given for the cast iron pan and the granite pan in Fig. 12c, d and e, f, respectively. As can be seen from these figures, the conduction time of the diode increases with the decrease in the coverage ratio as in the stainless-steel pan case. In case of 25% coverage with cast iron pan, V_{CEmax} , T_D and T_{DC-DC} values increased by 8, 50%, 133, 33% and 12, 50%, respectively. In case of 25% coverage with granite pan, V_{CEmax} , T_D and T_{DC-DC} values increased by 7, 84%, 75, 80% and 13, 80%, respectively. These results confirm the results obtained by simulation. It is seen that the amount of change in T_D is much more than the

other parameters. Therefore, determining the coverage ratio using the T_D value can be done sensitively.

7 Conclusion

In this study, a performance evolution of pan detection methods for SSQR inverter topology used in domestic induction heating is undertaken. Three different pans that have different ferromagnetic specifications are analyzed depending on pan position and power control methods. The main purpose is to determine the safe working limits for all kind of pans that can be used in induction hob system. Firstly, the theoretical analysis of the proposed pan detection methods has been carried out with simulations and the results are verified with experimental results. Six different pan detection methods have been used to understand the pan relative position, regardless of the control method and pan specifications. It is found out that the most effective way to understand load changing is T_D value change ratio at constant I_{LEQmax} . The aim of this study is to ensure that the change in the ferromagnetic structure is reliably detected by microcontroller-based control systems and that the system continues to operate safely. Pan detection methods used to understand the pan relative position are seemed to be one of the promising areas within induction cooking research field. This study may trigger further works to increase performance/costs ratio.

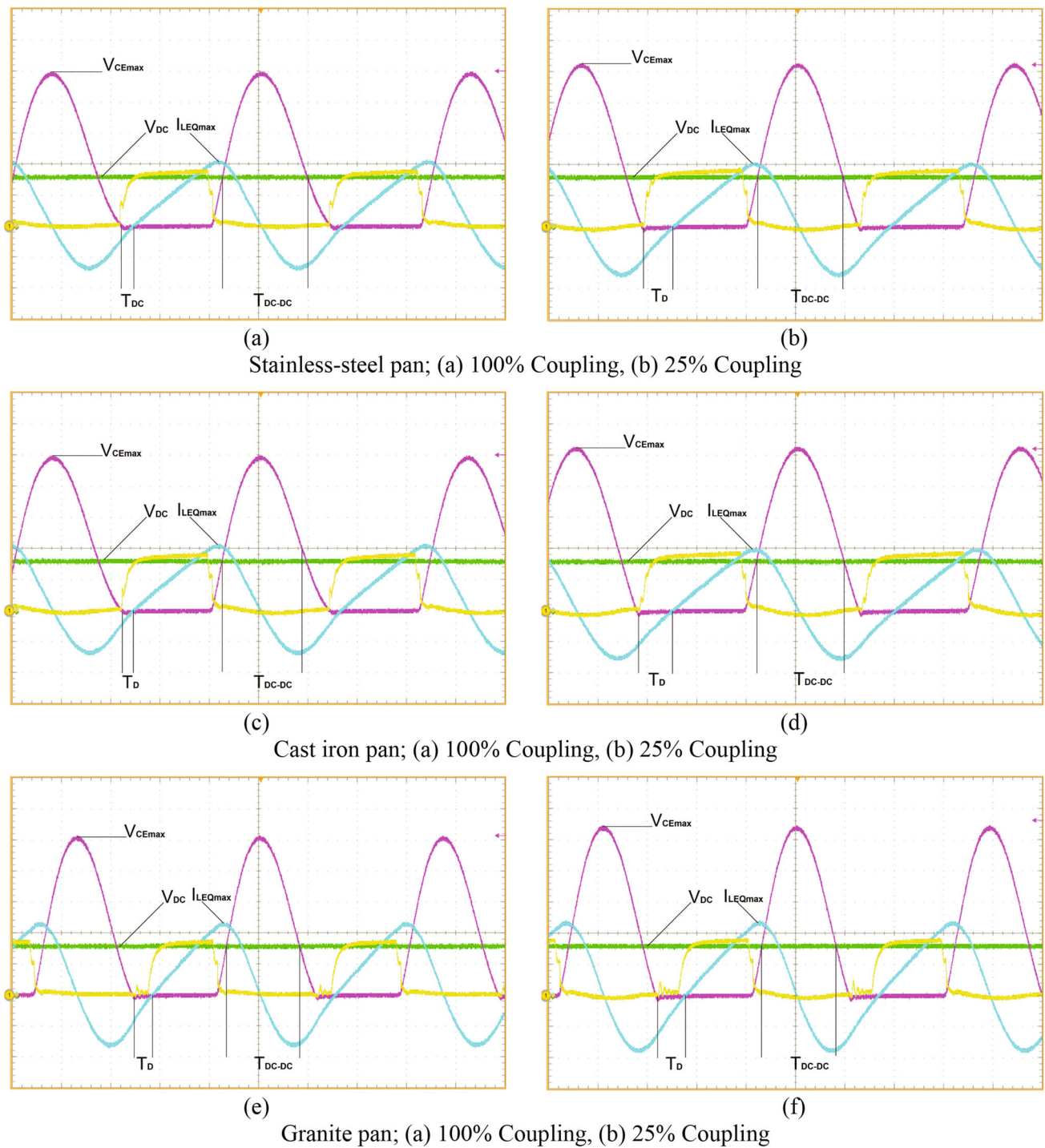


Fig. 12 Blue signal: I_{LEQ} coil current (20A/div), green signal: V_{DC} dc bus voltage (200 V/div), purple signal: V_{CE} collector voltage (200 V/div), yellow signal: V_{GE} gate voltage (10 V/div), time (10 μ s/div) (color figure online)

References

1. Sarnago H, Lucia O, Mediano A, Burdío JM (2014) A class-E direct AC–AC converter with multicycle modulation for induction heating systems. *IEEE Trans Ind Electron* 61(5):2521–2530
2. Geetha V, Sivachidambaranathan V (2020) Performance evaluation of half bridge AC–AC resonant converter by using various load in domestic purpose of induction heating application. *J Ambient Intell Hum Comput* 12:7085–7093
3. Llorente S, Monterde F, Burdío JM, Acero J (2002) A comparative study of resonant inverter topologies used in induction cookers. In: APEC 17th annual IEEE applied power electronics conference and exposition. Dallas, TX, USA
4. Tulu M. E, Yildirim D (2013) Induction cooker design with quasi resonant topology using jitter drive method. In: IEEE 12th international conference on environment and electrical engineering, Wroclaw, Poland
5. Lucia O, Burdío JM, Millan I, Acero J, Puyal D (2009) Load-adaptive control algorithm of half-bridge series resonant inverter for domestic induction heating. *IEEE Trans Ind Electron* 56(8):3106–3116
6. Sazak B. S, Cetin S (2009) Reducing the number of measurements in induction cooker design. In: IEEE 9th international conference on electronic measurement & instruments, Beijing, China
7. Acero J, Alonso R, Barragán LA, Burdío JM (2006) Modeling of planar spiral inductors between two multilayer media for induction heating applications. *IEEE Trans Magn* 42(11):3719–3729
8. Carretero C, Acero J, Alonso R, Burdío JM, Monterde F (2007) Temperature influence on equivalent impedance and efficiency of inductor systems for domestic induction heating appliances. in: APEC 07–22th annual IEEE applied power electronics conference and exposition. Anaheim, CA, USA
9. Ozturk M, Oktay U, Yilmaz N, Yardibi HS, Sinirlioglu S (2020) Comparison of pan detection methods for single switch topology used in domestic induction cooking. In: IEEE/SEST international conference on smart energy systems and technologies, Istanbul, Turkey
10. Park HP, Jung JH (2018) Load-adaptive modulation of a series-resonant inverter for all-metal induction heating applications. *IEEE Trans Ind Electron* 65(9):6983–6993
11. Dominguez A, Otin A, Urriza I, Barragan LA, Navarro D (2014) Load identification of domestic induction heating based on particle swarm optimization. *IEEE/COMPEL Santander, Spain*
12. Tanaka T (1989) A new induction cooking range for heating any kind of metal vessels. *IEEE Trans Consum Electron* 35(3):635–641
13. Kilic VT, Unal E, Demir HV (2016) Wireless metal detection and surface coverage sensing for all-surface induction heating. *Sensors* 16(3):363
14. Lucia O, Navarro D, Guillen P, Sarnago H, Lucia S (2019) Deep learning-based magnetic coupling detection for advanced induction heating appliances. *IEEE Access* 7:181668–181677
15. Villa J, Barragan LA, Artigas JI, Navarro D, Dominguez A, Cabeza T (2020) SoC-based in-cycle load identification of induction heating appliances. *IEEE Trans Ind Electron* 68(8):6762–6772
16. Acero J, Carretero C, Millán I, Lucía O, Alonso R, Burdío JM (2011) Analysis and modeling of planar concentric windings forming adaptable-diameter burners for induction heating appliances. *IEEE Trans Power Electron* 26(5):1546–1558
17. Villa J, Navarro D, Dominguez A, Artigas JI, Barragan LA (2021) Vessel recognition in induction heating appliances—a deep-learning approach. *IEEE Access* 9:16053–16061
18. Jimenez O, Lucia O, Barragan LA, Navarro D, Artigas JI, Urriza I (2014) FPGA-based test-bench for resonant inverter load characterization. *IEEE Trans Ind Inf* 9(3):1645–1654
19. Sarnago H, Lucia O, Burdío JM (2017) A versatile resonant tank identification methodology for induction heating systems. *IEEE Trans Power Electron* 33(3):1897–1901
20. Jimenez O, Lucia O, Urriza I, Barragan LA, Navarro D (2014) Analysis and implementation of FPGA-based online parametric identification algorithms for resonant power converters. *IEEE Trans Ind Inf* 10(2):1144–1153
21. Jimenez O, Barragan L. A, Navarro D, Artigas J. I, Urriza I, Lucia O (2011) FPGA-based harmonic computation through 1-bit data stream signals from delta-sigma modulators applied to induction heating appliances. In: IEEE applied power electronics conference and exposition, pp 1776–1781
22. Sarnago H, Lucia O, Burdío JM (2018) FPGA-based resonant load identification technique for flexible induction heating appliances. *IEEE Trans Ind Electron* 65(12):9421–9428
23. Li ZF, Hu JC, Huang MS, Lin YL, Lin CW, Meng YM (2022) Load estimation for induction heating cookers based on series RLC natural resonant current. *MDPI Energies* 15(4):1294
24. Bono-Nuez A, Martin-Del-Brio B, Bernal-Ruiz C, Pere-Cebolla FJ, Martinez-Iturbe A, Sanz-Gorrrachategui I (2018) The inductor as a smart sensor for material identification in domestic induction cooking. *IEEE Sens J* 18(6):2462–2470
25. Ozturk M, Zungor F, Emre B, Oz B (2022) Quasi resonant inverter load recognition method. *IEEE Access* 10:89376–89386
26. Jimenez O, Lucia O, Urriza I, Barragan LA, Navarro D (2014) Power measurement for resonant power converters applied to induction heating applications. *IEEE Trans Power Electron* 29(12):6779–6788
27. Sarnago H, Lucia O, Navarro D, Burdío JM (2015) Operating conditions monitoring for high power density and cost-effective resonant power converters. *IEEE Trans Power Electron* 31(1):488–496
28. Dominguez A, Barragan LA, Otin A, Navarro D, Puyal D (2014) Inverse-based power control in domestic induction-heating applications. *IEEE Trans Ind Electron* 61(5):2612–2621
29. Jimenez O, Lucia O, Urriza I, Barragan LA, Navarro D (2014) Design and evaluation of a low-cost high-performance $\Sigma - \Delta$ ADC for embedded control systems in induction heating appliances. *IEEE Trans Ind Electron* 61(5):2601–2611
30. Jimenez O, Lucia O, Urriza I, Barragan A, Mattavelli P, Boroyevich D (2014) An FPGA-based gain-scheduled controller for resonant converters applied to induction cooktops. *IEEE Trans Power Electron* 29(4):2143–2152
31. Sheikhan I, Kaminski N, Voß S, Scholz W, Herweg E (2013) Optimisation of quasi-resonant induction cookers. In: IEEE/EPE 15th European conference on power electronics and applications, Lille, France
32. Oh YS, Yeon JE, Cho KM, Kim HJ (2017) Resonant VLT of single-ended resonant inverter for induction heating. *IET Electron Lett* 53(12):804–806
33. Komatsu WPW (1998) A simple and reliable class E inverter for induction heating applications. *Int J Electron* 84(2):157–165

Publisher's Note Springer Nature remains neutral with regard to jurisdictional claims in published maps and institutional affiliations.

Springer Nature or its licensor (e.g. a society or other partner) holds exclusive rights to this article under a publishing agreement with the author(s) or other rightsholder(s); author self-archiving of the accepted manuscript version of this article is solely governed by the terms of such publishing agreement and applicable law.